AGU PUBLICATIONS

Geophysical Research Letters

RESEARCH LETTER
10.1002/2015GL066481

Key Points:
- Submerged blocks of eroded bank material directly affect the 3-D near-bank flow field
- Submerged slump blocks may deflect flow onto the bank
- A new conceptual model of bank erosion accounts for the influence of submerged slump blocks

Supporting Information:
- Figures S1–S6, Captions for Movies S1–S4, and Text S1
- Movie S1
- Movie S2
- Movie S3
- Movie S4

Correspondence to:
C. Hackney,
C.R.Hackney@soton.ac.uk

Citation:
Hackney, C., J. Best, J. Leyland, S. E. Darby, D. Parsons, and R. Aalto (2015), Modulation of outer bank erosion by slump blocks: Disentangling the protective and destructive role of failed material on the three-dimensional flow structure, *Geophys. Res. Lett., 42*, 10,663–10,670, doi:10.1002/2015GL066481.

Received 6 OCT 2015
Accepted 17 NOV 2015
Accepted article online 24 NOV 2015
Published online 19 DEC 2015

Modulation of outer bank erosion by slump blocks: Disentangling the protective and destructive role of failed material on the three-dimensional flow structure

Christopher Hackney[1], Jim Best[2], Julian Leyland[1], Stephen E. Darby[1], Daniel Parsons[3], Rolf Aalto[4], and Andrew Nicholas[4]

[1]Geography and Environment, University of Southampton, Southampton, UK, [2]Department of Geology, Department of Geography and GIS, Department of Mechanical Science and Engineering, and Ven Te Chow Hydrosystems Laboratory, University of Illinois at Urbana-Champaign, Urbana, Illinois, USA, [3]Geography, Earth and Environmental Sciences, University of Hull, Hull, UK, [4]University of Exeter, Exeter, UK

Abstract The three-dimensional flow field near the banks of alluvial channels is the primary factor controlling rates of bank erosion. Although submerged slump blocks and associated large-scale bank roughness elements have both previously been proposed to divert flow away from the bank, direct observations of the interaction between eroded bank material and the 3-D flow field are lacking. Here we use observations from multibeam echo sounding, terrestrial laser scanning, and acoustic Doppler current profiling to quantify, for the first time, the influence of submerged slump blocks on the near-bank flow field. In contrast to previous research emphasizing their influence on flow diversion away from the bank, we show that slump blocks may also deflect flow onto the bank, thereby increasing local shear stresses and rates of erosion. We use our measurements to propose a conceptual model for how submerged slump blocks interact with the flow field to modulate bank erosion.

1. Introduction

The erosion and deposition of sediment by fluvial bank erosion plays a pivotal role in maintaining the ecological and geomorphological diversity of fluvial channels [*Florsheim et al.*, 2008; *Camporeale et al.*, 2013]. Previous research has shown how the rate at which sediment is exhumed from floodplains by the processes of bank failure, sediment entrainment, and transportation has far reaching implications for geomorphology, ecology, infrastructure management, and nutrient and contaminant tracking [e.g. *Marron*, 1992; *Reneau et al.*, 2004; *O'Neal and Pizzuto*, 2011; *Zinger et al.*, 2011]. The intricate relationship between the erosive forces of hydraulic bank erosion (i.e., fluid shear stress) and the 'resistive' forces, as controlled by the lithology and morphology of the bank, make a full appreciation of the flow-form interactions at the river bank a prerequisite to understanding, and predicting, rates of bank erosion.

Past work has highlighted the role of submerged blocks of eroded bank material (henceforth 'slump blocks') in modifying the near-bank flow structure, by providing protective material to the base of the bank [*Thorne*, 1982; *Wood et al.*, 2001; *Parker et al.*, 2011] as well as increasing bank roughness, thereby diverting high-velocity flows away from the bank [*Motta et al.*, 2014]. Bank roughness is further enhanced by the bankline topography, which becomes embayed as bank failures occur [*Kean and Smith*, 2006a, 2006b]. In studies of bank erosion within actively migrating meandering channels, recent research has proposed that cohesive slump blocks may serve to armor the underlying noncohesive bed and thus reduce bank erosion [*Dulal et al.*, 2010; *Parker et al.*, 2011; *Asahi et al.*, 2013; *Eke et al.*, 2014]. *Parker et al.* [2011] argue that subsequent breakdown of the slump blocks may diminish protection of the river bank and lead to renewed bank failure and slumping. *Motta et al.* [2014] also find that slump blocks may protect the bank from erosion, with slump block size, bank height and slope, river bed topography, and the presence/type of vegetation potentially controlling their influence on the near-bank processes. However, as detailed observations of the 3-D flow field around, and through, these roughness elements are currently lacking, these models remain largely untested.

Although past studies have investigated the effect of bank roughness on near-bank flows, these have either been of insufficient spatial resolution to resolve fully the three-dimensional flow near the bank [*Jin et al.*, 1990; *Thorne and Furbish*, 1995], or they have documented flow associated with large-scale roughness elements in

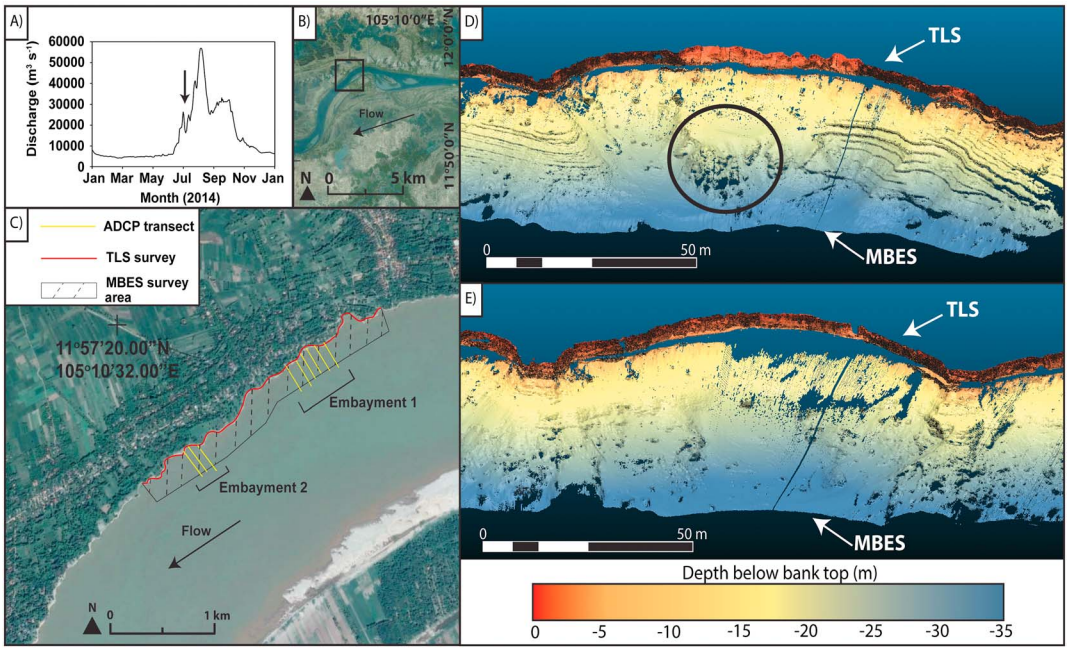

Figure 1. (a) The 2014 hydrograph of the Mekong River at Kratie, Cambodia. Surveys were conducted at the time highlighted by the arrow. (b) Location of the study site on the outer bank of a large meander, located ~150 km downstream of the gauge at Kratie. (c) The location of flow and topographic data sets used in this study. The yellow lines depict acoustic Doppler current profiler (ADCP) transects, whereas the red line depicts the extent of the terrestrial laser scanner (TLS) survey undertaken. The shaded box outlines the area covered by the multibeam echosounding (MBES) survey. The two bank embayments discussed in this paper are highlighted. (d) Embayment 1 topography, representative of a newly formed embayment. (e) Embayment 2 topography, which is a more developed (older) embayment. Note the slump block highlighted by the black circle in Figure 1d and the lack of failed material along the bank toe in Figure 1e. Flow is right to left in each of Figures 1d and 1e.

physical experiments [*Mizumura and Yamasaka*, 2002; *McCoy et al*., 2007, 2008; *Yossef and de Vriend*, 2011] and numerical models [*Mcbride et al*., 2007; *Blanckaert et al*., 2010, 2012, 2013; *Abad et al*., 2013], or studied the effects of artificial bend-way weirs, wing-dikes, and groins [*Abad et al*., 2008; *Jamieson et al*., 2011]. The current absence of detailed 3-D measurements documenting the effects of bank roughness on near-bank flow in natural channels is partly due to the complexity and spatial scale of the processes involved and remains a significant research gap [*Motta et al*., 2014]. Resolving the 3-D flow field and obtaining high-resolution topographic data at the scale of the roughness elements in the near-bank region has long been a challenge. However, recent advances in acoustic Doppler profiling [*Kostaschuk et al*., 2005; *Szupiany et al*., 2007, 2009; *Vermeulen et al*., 2014] and high-resolution topographic data collection [*Parsons et al*., 2005; *Aalho et al*., 2009; *Nittrouer et al*., 2011; *Lotsari et al*., 2014; *Kasvi et al*., 2015; *Leyland et al*., 2015] now enable the instantaneous flow and morphology of the near-bank region to be fully quantified, allowing for the novel investigation of these complex process-form interactions.

Herein we report on unique data from the Mekong River, Cambodia, obtained using a suite of high-resolution topographic (terrestrial laser scanner and multibeam echo sounder) and flow (acoustic Doppler current profiler) instrumentation that quantify the topography and 3-D flow structure within embayments situated on the outer bank of a large meander bend. Our data reveal, for the first time, the complex flow-form interactions that occur around these large-scale roughness elements and highlight how slump blocks may initially enhance bank erosion, through their steering of the 3-D flow field, before the role of larger bank embayments and large-scale outer bank flow separation act to reduce erosion rates. We use our observations to propose a new conceptual model for the role of bank roughness in controlling the evolution of bankline topography and hence modulating rates of bank erosion.

2. Study Site

We present observations from the outer bank of a meander bend (radius of curvature ~3500 m) on the Mekong River, Cambodia (Figure 1). The Mekong River ranks 12th, globally, in terms of its length (4900 km)

and tenth in terms of its mean annual runoff (475 km^3) [*Mekong River Commission*, 2005]. This runoff drives a mean annual sediment load of *c*. 1.6×10^8 t [*Milliman and Meade*, 1983]. The study site is located in a reach that migrates freely across largely Quaternary alluvium [*Gupta and Liew*, 2007; *Kummu et al*., 2008; *Carling*, 2009]. The banks at the study site are between 15 and 20 m in height, locally reaching up to 30 m, are formed of homogenous, erodible, unconsolidated, silty, alluvium ($D_{50} = 6.2$ μm), with the critical shear stress of the bank material being 0.6 N m^{-2} ($\sigma = 0.3$ N m^{-2}, see supporting information for more details of how this estimate was obtained).

3. Methods

Measurements of the bank and near-bank topography, for both the submerged and emergent portions of the banks, were made simultaneously from a vessel using a Reson SeaBat 7125SV multibeam echosounder (MBES) and a Leica P20 terrestrial laser scanner (TLS). Briefly, both instruments were located together spatially and temporally using a Leica 1230 differential Global Positioning System (dGPS) in Real-Time Kinematic (RTK) mode, which produced an accuracy in relative position (dGPS base station to vessel antenna) of ±0.02 m in the horizontal and vertical positions. The dGPS was coupled to an Applanix POS-MV WaveMaster inertial motion unit that also provided full, real-time, 3-D motion and heading data correction for both MBES and TLS, along with the synchronization of all survey data streams using the dGPS time stamp and a pulse per second (PPS) signal. The survey data were synchronized and collected using QPS Quality Integrated Navigation System software. Postsurvey calibration and correction for angular offsets and the application of sound velocity corrections were applied to the MBES data within CARIS-HIPS software.

Simultaneous with the topographic survey, detailed 3-D flow fields of the near-bank flow structure were measured using an RDI Teledyne 600 kHz acoustic Doppler current profiler (ADCP) deployed from a second vessel. Flow measurements were conducted along a series of short (200 m; ~0.2 of a channel width) transects set perpendicular to the average bank curvature (Figure 1c, and see supporting information, Figure S4, for more details). All flow surveys were conducted when the discharge was 23,000 m^{-3} s^{-1} (Figure 1a). The ADCP was coupled to the same RTK dGPS used in the topographic surveys to provide both position and velocity corrections of the survey vessel. Four passes were recorded along each transect to allow the time-averaged flow structure to be assessed [*Szupiany et al*., 2007], with individual passes giving an indication of the shorter-term, 'instantaneous', flow structure. The ADCP data were processed in the Velocity Mapping Toolbox (VMT) [*Parsons et al*., 2013]. The resultant mean transects were then rotated using the method of *Rozovskii* [1957] that has been shown to capture well details of the primary and secondary flow fields in a range of complex channel planforms [*Rhoads and Kenworthy*, 1995; *Lane et al*., 2000; *Szupiany et al*., 2009].

4. Observations

Our MBES and TLS surveys reveal that a series of distinct embayments and slump blocks dominate the subaqueous near-bank topography (Figures 1c, 1d, and 1e). These features can be up to 200 m in downstream length and 70 m in across-stream width (Figure 1c). Slump block size ranges from 20 × 15 × 10 m (across-stream × downstream × height dimensions) down to blocks that are only decimeters in size, creating a complex assemblage of roughness elements both near to the bank and extending out to *c*. 50 m from the bankface. It is noticeable that some slump blocks are relatively smaller than others and that the failed material is located closer to the bank toe in some embayments. This is due to the greater exposure of older failed material to extended periods of geomorphologically effective flow during which the blocks are trimmed, and material is removed from the bank toe [*Wood et al*., 2001].

Observations of the 3-D flow field from within an embayment (159 m in downstream length and 28 m in across-stream width) with a large slump block (Embayment 1, slump block circled in Figure 1d) highlight the dominance of both recirculating, separated, flow downstream of the upstream point of the embayment (Figure 2a) and upwelling, bank-directed, flow around the large slump block itself (Figure 2c). It is noted (Figures 2b and 2c) that the slump block is located at the outer edge of the recirculation zone that has formed in the embayment. Time-averaged ADCP data reveal that recirculating flow (of *c*. -0.4 m s^{-1}) is created within the embayment. Flow at the surface recirculates within the embayment and reattaches to the bank near the downstream limit of the embayment. In addition, flow is steered toward the bank by the large slump block that generates an upwelling in its downstream leeside (Figures 2b and 2c). Time-averaged smoothed

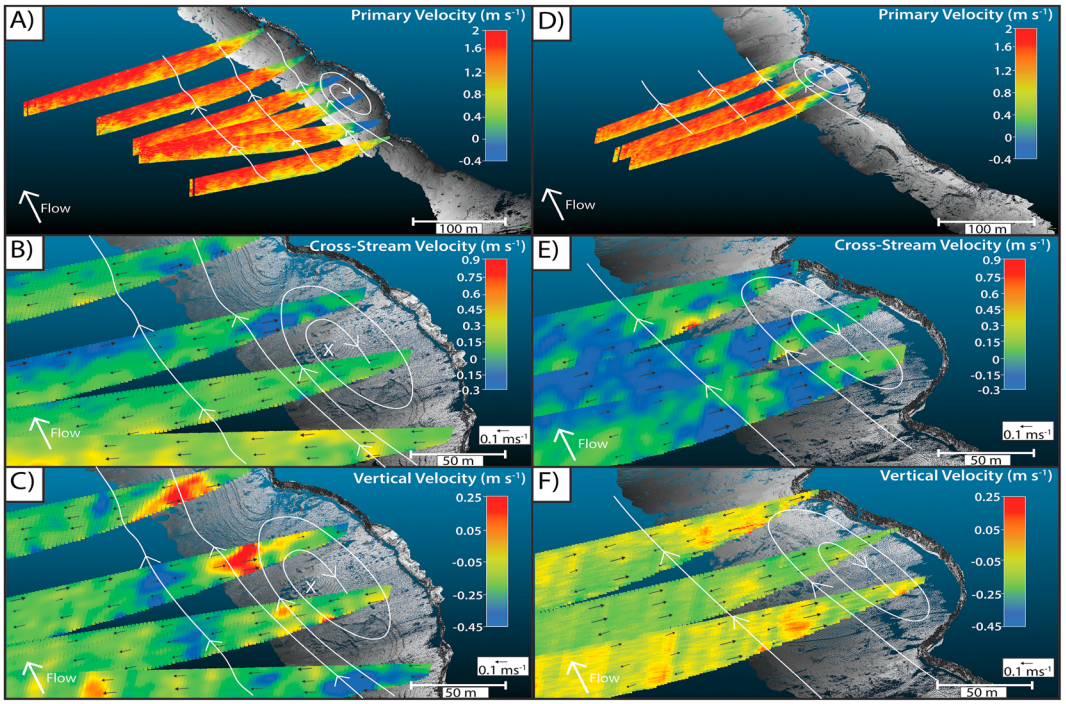

Figure 2. The 3-D flow structure observed within the bank embayments (Embayment 1: a–c) with slump blocks and (Embayment 2: d–f) without slump blocks. Figures 2a and 2c display primary flow velocity (m s^{-1}) after rotation following the method of *Rozovskii* [1957]. Streamlines of primary velocity are depicted as white lines in all panels. Figures 2b and 2e display cross-stream flow velocity (m s^{-1}; where blue is flow into the bank, red is flow away from the bank) as defined by *Rozovskii* [1957]. Figures 2c and 2f display vertical flow velocities (m s^{-1}) where red is upwelling and blue is downwelling. Note color scales vary between panels. The black arrows in Figures 2b, 2c, 2e, and 2f are cross-stream velocity vectors, scaled by magnitude. The cross in Figures 2b and 2c mark the location of the slump block highlighted in Figure 1 and discussed in the text.

ADCP data highlight upwelling (0.25 m s^{-1}) over the slump block (Figure 2c), although instantaneous upwelling, captured in an individual ADCP cross section, may reach up to 0.4 m s^{-1} (see Figure S5 in the supporting information). Flow is seen to be diverted strongly toward the bank in the lee of the slump block, with bankward flow velocities of 0.3 m s^{-1} (Figure 2b). At this embayment, flow is thus beginning to form a near-bank dead zone where flow velocities are lower (−0.4 m s^{-1} near the bank compared to 2 m s^{-1} at a distance of ~200 m away from the bank) and thus may serve to reduce the rates of bank erosion. However, at the downstream termination of this flow separation zone, both flow reattachment and flow steering by the slump block bring high-velocity fluid inward toward the bank, generating upwelling and yielding higher-boundary shear stresses in the lee-side of the slump block (Figure 3a). The combined effects of flow reattachment from large-scale recirculation in the evolving embayment and topographic steering of flow around the slump block therefore focus the location of erosion at the downstream limit of the embayment, suggesting that the embayment will continue to enlarge and migrate in the downstream direction.

Conversely, observations of the 3-D flow field from within an embayment (114 m in downstream length and 24 m in across-stream width) without failed material at the bank toe (Embayment 2 and Figure 1e) reveal that the flow is dominated solely by recirculating flow. The zone of recirculating flow encompasses the entire length and width of the embayment (Figure 2d) and, although the upstream flow in this recirculation zone is similar in magnitude to that observed in Embayment 1, instantaneous maximum recirculating flow velocities were recorded of −0.8 m s^{-1} compared to −0.4 m s^{-1}, thus providing an extensive area of low velocities that may serve to decrease boundary shear stresses (Figure 3b). The reattachment point is located at the downstream limit of the embayment, and here higher boundary shear stresses are present as flow impinges against the bank (Figure 3b). It is noted that this embayment is located downstream of a series of embayments (Figure 1c), and there may thus be some flow inheritance and influence on the primary and secondary flow. The lack of failed material in the subaqueous topography results in lower-magnitude (relative to Embayment 1) vertical velocities

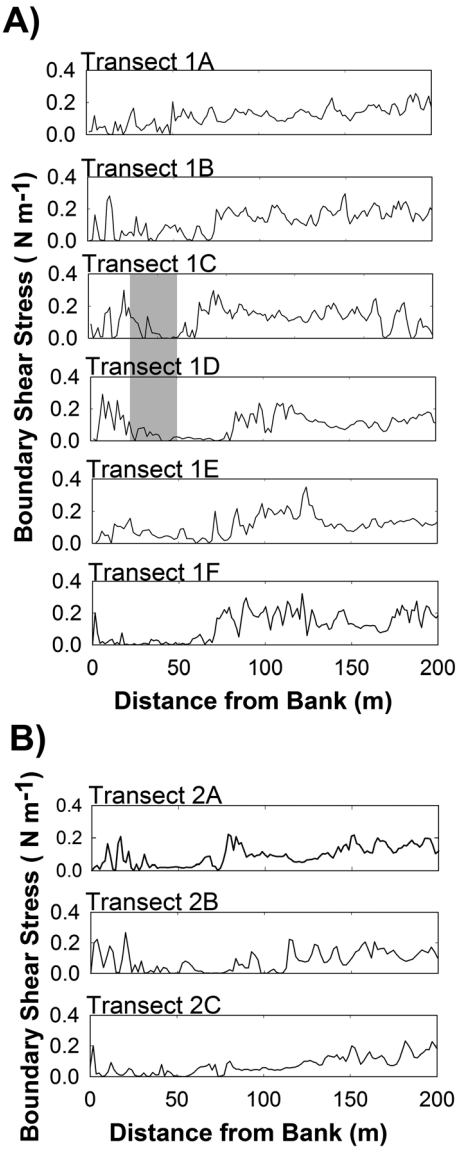

Figure 3. (a) Boundary shear stress (N m^{-2}) derived from the time-averaged ADCP transects within Embayment 1. The grey boxes in Transects 1C and 1D denote the extent of the slump block in the cross-stream dimension (see Figure 1d). The block is located 20 m upstream of Transect 1C and 10 m downstream of Transect 1D. In total, the block is 25 m in downstream length. Note how the location of peak shear stress close to the bank is deflected away from the bank at the entrance to the embayment (transects 1B and 1C), but is located much closer to the bank in transect 1D. A smaller peak in boundary shear stresses occurs in Transect 1 F, at the downstream extent of the embayment, due to flow reattachment. (b) Boundary shear stress (N m^{-2}) derived from the time-averaged ADCP transects within Embayment 2 without slump blocks. Note how the distribution of shear stresses close to the bank remains constant in location through the embayment. The peak in boundary shear stresses in Transect 2C, at the downstream extent of the embayment, represents the flow reattachment zone.

(Figure 2f), both in the time averaged (0.1 m s^{-1} compared to 0.25 m s^{-1}) and instantaneous (0.2 m s^{-1} compared to 0.4 m s^{-1}) ADCP cross sections (see supporting information Figure S6). The reduced magnitude and extent of this near-bank upwelling reduces boundary shear stresses when compared to those experienced in the presence of a slump block (Figure 3).

5. Discussion

The application of high-resolution 3-D flow and topographic survey techniques to bank embayments at different stages of their evolution has revealed the influence that slump blocks may have upon the instantaneous near-bank flow field. Our observations reveal that, at certain phases during the lifetime of slump blocks, the near-bank flow field may be deflected up and over the block and toward the bank, thereby promoting erosion. In a similar way, observations have shown that flow may be deflected up and over bendway weirs and groines at certain flow stages [*Abad et al.*, 2008; *McCoy et al.*, 2008; *Bhuiyan et al.*, 2010; *Jamieson et al.*, 2011; *Yossef and de Vriend*, 2011]. *Abad et al.* [2008] found that flow over submerged bendway weirs at bankfull and half bankfull stage steered flow over these structures, accelerating flow around them and leading to higher shear velocities due to flow acceleration over, and fluid shear from, the tips of the weirs (by way of comparison, our study was conducted at half the bankfull discharge). *Abad et al.* [2008] also found that although such weirs could help reduce bank erosion by reducing basal scour, flow around the weirs at higher flow stages could promote bank retreat due to increased shear stresses on the bank produced by the weir flow field. These results find similarities in the slump block flow fields revealed herein.

Previous treatments of slump blocks in models of outer bank erosion and channel migration have been grounded in a 1-D/2-D representation of the role that roughness plays in diverting the high-velocity core away from the bank through the influence of form drag [*Kean and Smith*, 2006a, 2006b], as well as the protective role of failed material at the bank toe [*Parker et al.*, 2011; *Motta et al.*, 2014]. These approaches have led to a treatment of the armoring afforded by failed material within models of meandering river migration, such that as the block disintegrates, the level of protection provided to the bank toe decreases linearly [e.g. *Parker et al.*, 2011]. Indeed, *Eke et al.* [2014] highlight that an explicit treatment of the role that slump blocks play in influencing bank shear stresses is missing from the current model of *Parker et al.* [2011]. The data presented herein demonstrates that such a relationship may be more complex than current representations of this phenomenon suggest, in that at different periods of slump block evolution, near-bank shear stresses may

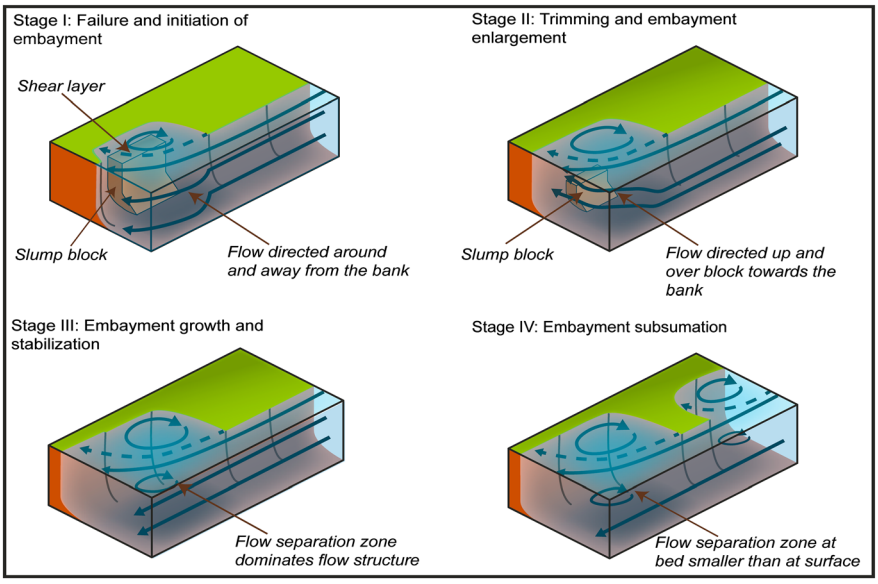

Figure 4. Conceptual model for the development of a bank embayment and the role that slump blocks play in diverting flow away from, and on to, the bank at different stages of embayment evolution. The black lines represent streamlines. The dashed lines represent the shear layer.

be increased, as well as decreased, as a direct result of blocks of failed material. Although in some configurations early in their life cycle, slump blocks may deflect high-velocity cores away from the bank, thus reducing bank shear stresses [*Kean and Smith*, 2006a, 2006b; *Parker et al*., 2011], our results show that once the block has been trimmed sufficiently, slump blocks may steer flow up, over, and around their topography and onto the adjacent bank. This flow deflection increases boundary shear stresses, focusing erosion onto the downstream end of the block and near the end of the bank embayment. We note that this mechanism may also occur where slump blocks exist in the absence of embayments and that additional further studies are required at a range of spatial scales to ascertain whether this behavior is scale dependent. Such effects also find parallels in the recent work of *Abad et al*. [2013] who document the influence of migrating bedforms on bank shear stresses. A fruitful avenue for future studies will be to better quantify the turbulent fluxes and Reyonlds stresses associated with these slump block effects. Nevertheless, such flow-steering due to slump block topography has clear implications for the rate, and location, of erosion as represented in numerical models of bank erosion.

The present study thus highlights the need to better constrain the role that slump blocks and embayments play in bank erosion, since these roughness elements play a key role in determining the rates and mechanisms of channel migration through their role in driving chute cutoffs [*Markham and Thorne*, 1992; *Constantine et al*., 2010; *Grenfell et al*., 2012] and moderating rates of bank erosion [*Kean and Smith*, 2006a, 2006b; *Darby et al*., 2010; *Leyland et al*., 2015]. Our results now enable the added complexity of form-flow interactions produced by the presence of slump blocks to be incorporated into these models. To this end, we propose a new conceptual model for the evolution of river bank embayments (Figure 4) that accounts for both the protective role afforded by slump blocks in their early stages and the enhanced erosion they may induce due to topographic steering at later stages of their evolution.

During Stage I (Figure 4), a single, or series of, bank failures causes the formation of the initial embayment and the deposition of failed material at the bank toe. At this stage, the high-velocity core is deflected away from the bank toe by the failed material and planform geometry of the embayment, thus affording protection to the bank. In Stage II, hydraulic forces act to erode and trim the slump block. Although form roughness induced by the larger planform of the bank continues to deflect high-velocity cores away from the bank, topographic steering of the near-bank flow causes flow to move over, and around, the block, generating bank-directed flow. This flow steering causes higher shear stresses to be exerted on the bank and leads to downstream enlargement of the embayment. Erosion also occurs due to the high shear stresses present in the reattachment region of the flow separation zone formed within the embayment. Stage III sees growth of the embayment and the continued disintegration of the slump block, with further slumps adding to

erosion as in Stage II. The embayment grows in size, increasing form drag, until it generates a sustained large zone of recirculating, separated, flow that is larger than any new slumps that move into this region. Slower flow within the majority of the larger flow separation region produces lower velocities, which lessen bank erosion, with erosion now principally occurring at the downstream end of the embayment. Finally, Stage IV sees the embayment size stabilize due to large-scale flow separation protecting the bank from significant further erosion. The development of upstream embayments, formed from new slumps, may propagate downstream and subsume the original embayment, returning the bankline to a preembayment planform.

In summary, the role of submerged slump blocks in modulating the near-bank 3-D flow field is far more complex than previously thought. Failed material may act to both protect the bank from erosion as proposed in past work [*Wood et al*., 2001; *Parker et al*., 2011; *Motta et al*., 2014] but may also enhance bank erosion by deflecting flow up, and onto, the bank as the geometric properties of the slump block change. It is thus clear that in order to develop better predictive models of bank erosion, all of these effects must be considered, and that future work needs to parameterize the influence of slump block flow-form interactions at different stages of embayment evolution. Although the present results illustrate one case example, our novel data suggest the possible differential influences of slump blocks at various times in their life cycle. Further research is needed to constrain these process dynamics across a range of flow stages that determine the magnitude and distribution of shear stress [*Papanicolaou et al*., 2007; *Guo and Julien*, 2009; *Nikora and Roy*, 2012]. Additionally, more work is needed to quantify the effects of slump block size, orientation, shape and position relative to the bank, and their role in enhancing or reducing bank erosion, in a similar way to past studies of flow around groins and bendway weirs [*Przedwojski*, 1995; *Abad et al*., 2008].

Acknowledgments

This research was supported by awards NE/JO21970/1, NE/JO21571/1, and NE/JO21881/1 (to Southampton, Exeter, and Hull, respectively) from the UK Natural Environment Research Council (NERC). J.B. was in receipt of a Diamond Jubilee Fellowship from the University of Southampton and a National Great Rivers Research and Education Center (NGRREC) Faculty Fellowship that facilitated the writing of this paper. All data are available on request from the corresponding author. We thank the Mekong River Commission and Department for Hydrology and Water Resources in Cambodia for logistical support. We thank Mark Dover of the Cartographic Unit, Geography and Environment, University of Southampton for his help in producing Figure 4. The comments of the editor and two reviewers greatly improved the quality of the manuscript.

References

Aalho, P., A. Hyyppa, H. Kaartinen, J. Hyyppa, and A. Jaakkola (2009), Application of boat-based laser scanning for river survey, *Earth Surf. Processes Landforms*, *34*, 1831–1838, doi:10.1002/esp.1879.

Abad, J. D., B. L. Rhoads, I. Güneralp, and M. H. Garcia (2008), Flow structure at different stages in a meander-bend with bendway weirs, *J. Hydraul. Eng.*, *134*, 1052–1063.

Abad, J. D., C. E. Frias, G. C. Buscaglia, and M. H. Garcia (2013), Modulation of the flow structure by progressive bedforms in the Kinoshita meandering channel, *Earth Surf. Processes Landforms*, *38*(13), 1612–1622, doi:10.1002/esp.3460.

Asahi, K., Y. Shimizu, J. Nelson, and G. Parker (2013), Numerical simulation of river meandering with self evolving banks, *J. Geophys. Res. Earth Surf.*, *118*, 2208–2229, doi:10.1002/jgrf.20150.

Bhuiyan, F., R. D. Hey, and P. R. Wormleaton (2010), Bank-attached vanes for bank erosion control and restoration of river meanders, *J. Hydraul. Eng.*, *136*(9), 583–596, doi:10.1061/(ASCE)HY.1943-7900.0000217.

Blanckaert, K., A. Duarte, and A. J. Schleiss (2010), Influence of shallowness, bank inclination and bank roughness on the variability of flow patterns and boundary shear stress due to secondary currents in straight open-channels, *Adv. Water Resour.*, *33*(9), 1062–1074, doi:10.1016/j.advwatres.2010.06.012.

Blanckaert, K., A. Duarte, Q. Chen, and A. J. Schleiss (2012), Flow processes near smooth and rough (concave) outer banks in curved open channels, *J. Geophys. Res.*, *117*, F04020, doi:10.1029/2012JF002414.

Blanckaert, K., M. G. Kleinhans, S. J. McLelland, W. S. J. Uijttewaal, B. J. Murphy, A. van de Kruijs, D. R. Parsons, and Q. Chen (2013), Flow separation at the inner (convex) and outer (concave) banks of constant-width and widening open-channel bends, *Earth Surf. Processes Landforms*, *38*(7), 696–716, doi:10.1002/esp.3324.

Camporeale, C., E. Perucca, L. Ridolfi, and A. M. Gurnell (2013), Modeling the interactions between river morphodynamics and riparian vegetation, *Rev. Geophys.*, *51*, 379–414, doi:10.1002/rog.20014.

Carling, P. A. (2009), The geology of the Lower Mekong River, in *The Mekong: Biophysical Environment of an International River Basin*, edited by I. C. Campbell, pp. 13–28, Acaemic Press, New York.

Constantine, J. A., S. R. McLean, and T. Dunne (2010), A mechanism of chute cutoff along large meandering rivers with uniform floodplain topography, *Bull. Geol. Soc. Am.*, *122*(5–6), 855–869, doi:10.1130/B26560.1.

Darby, S. E., H. Q. Trieu, P. A. Carling, J. Sarkkula, J. Koponen, M. Kummu, I. Conlan, and J. Leyland (2010), A physically based model to predict hydraulic erosion of fine-grained riverbanks: The role of form roughness in limiting erosion, *J. Geophys. Res.*, *115*, F04003, doi:10.1029/2010JF001708.

Dulal, K. P., K. Kobayashi, Y. Shimizu, and G. Parker (2010), Numerical computation of free meandering channels with the application of slump blocks on the outer bends, *J. Hydro-environ. Res.*, *3*(4), 239–246, doi:10.1016/j.jher.2009.10.012.

Eke, E., G. Parker, and Y. Shimizu (2014), Numerical modelling of erosional and depositional bank processes in migrating river bends with self-formed width: Morphodynamics of bar push and bank pull, *J. Geophys. Res. Earth Surf.*, *119*, 1455–1483, doi:10.1002/2013JF003020.

Florsheim, J. L., J. F. Mount, and A. Chin (2008), Bank erosion as a desirable attribute of rivers, *BioScience*, *58*(6), 519–529.

Grenfell, M. C., R. Aalto, and A. Nicholas (2012), Chute channel dynamics in large, sand-bed meandering rivers, *Earth Surf. Processes Landforms*, *37*(3), 315–331, doi:10.1002/esp.2257.

Guo, J., and P. Y. Julien (2009), Shear stress in smooth rectangular open-channel flows, *J. Hydraul. Eng.*, *131*(1), 30–37, doi:10.1061/(ASCE)0733-9429(2005)131:1(30).

Gupta, A., and S. C. Liew (2007), The Mekong from satellite imagery: A quick look at a large river, *Geomorphology*, *85*(3–4), 259–274, doi:10.1016/j.geomorph.2006.03.036.

Jamieson, E. C., C. D. Rennie, R. B. Jacobson, and R. D. Townsend (2011), 3-D flow and scour near a submerged wing dike: ADCP measurements on the Missouri River, *Water Resour. Res.*, *47*, W07544, doi:10.1029/2010WR010043.

Jin, Y. C., P. M. Steffler, and F. E. Hicks (1990), Roughenss effects on flow and shear-stress near outside bank of curved channel, *J. Hydraul. Eng.*, *116*(4), 563–577, doi:10.1061/(ASCE)0733-9429(1990).

Kasvi, E., M. Vaaja, H. Kaartinen, A. Kukko, A. Jaakkola, C. Flener, H. Hyyppä, J. Hyyppä, and P. Alho (2015), Sub-bend scale flow–sediment interaction of meander bends—A combined approach of field observations, close-range remote sensing and computational modelling, *Geomorphology*, *238*, 119–134, doi:10.1016/j.geomorph.2015.01.039.

Kean, J. W., and J. D. Smith (2006a), Form drag in rivers due to small-scale natural topographic features: 1. Regular sequences, *J. Geophys. Res.*, *111*, F04009, doi:10.1029/2006JF000467.

Kean, J. W., and J. D. Smith (2006b), Form drag in rivers due to small-scale natural topographic features: 2. Irregular sequences, *J. Geophys. Res.*, *111*, F04010, doi:10.1029/2006JF000490.

Kostaschuk, R., J. Best, P. Villard, J. Peakall, and M. Franklin (2005), Measuring flow velocity and sediment transport with an acoustic Doppler current profiler, *Geomorphology*, *68*(1–2), 25–37, doi:10.1016/j.geomorph.2004.07.012.

Kummu, M., X. X. Lu, A. Rasphone, J. Sarkkula, and J. Koponen (2008), Riverbank changes along the Mekong River: Remote sensing detection in the Vientiane–Nong Khai area, *Quat. Int.*, *186*(1), 100–112, doi:10.1016/j.quaint.2007.10.015.

Lane, S. N., K. F. Bradbrook, K. S. Richards, P. M. Biron, and A. G. Roy (2000), Secondary circulation cells in river channel confluences: Measurement artefacts or coherent flow structures?, *Hydrol. Processes*, *14*, 2047–2071.

Leyland, J., S. E. Darby, L. Teruggi, M. Rinaldi, and D. Ostuni (2015), A self-limiting bank erosion mechanism? Inferring temporal variations in bank form and skin drag from high resolution topographic data, *Earth Surf. Processes Landforms*, doi:10.1002/esp.3739.

Lotsari, E., M. Vaaja, C. Flener, H. Kaartinen, A. Kukko, E. Kasvi, H. Hyyppä, J. Hyyppä, and P. Alho (2014), Annual bank and point bar morphodynamics of a meandering river determined by high-accuracy multitemporal laser scanning and flow data, *Water Resour. Res.*, *50*, 5532–5559, doi:10.1002/2013WR014106.

Markham, A. J., and C. R. Thorne (1992), Geomorphology of gravel-bed river bends, in *Dynamics of Gravel-Bed Rivers*, edited by P. Billi et al., pp. 433–457, Wiley, Chichester.

Marron, D. C. (1992), Floodplain storage of mine tailings in the Belle Fourche River system: A sediment budget approach, *Earth Surf. Processes Landforms*, *17*, 675–685, doi:10.1002/esp.3290170704.

Mcbride, M., W. C. Hession, D. M. Rizzo, and D. M. Thompson (2007), The influence of riparian vegetation on near-bank turbulence: A flume experiment, *Earth Surf. Processes Landforms*, *32*(13), 2019–2037, doi:10.1002/esp.

McCoy, A., G. Constantinescu, and L. Weber (2007), A numerical investigation of coherent structures and mass exchange processes in channel flow with two lateral submerged groynes, *Water Resour. Res.*, *43*, W05445, doi:10.1029/2006WR005267.

McCoy, A., G. Constantinescu, and L. J. Weber (2008), Numerical investigation of flow hydrodynamics in a channel with a series of groynes, *J. Hydraul. Eng.*, *134*(2), 157–172, doi:10.1061/(ASCE)0733-9429(2008)134:2(157).

Mekong River Commission (2005), *Overview of the Hydrology of the Mekong River Basin*, Mekong River Commission, Vientiane, Laos.

Milliman, J. D., and R. H. Meade (1983), World-wide delivery of river sediment to the oceans, *J. Geol.*, *91*(1), 1–21.

Mizumura, K., and M. Yamasaka (2002), Flow in open-channel embayments, *J. Hydraul. Eng.*, *128*, 1098–1101.

Motta, D., E. J. Langendoen, J. D. Abad, and M. H. García (2014), Modification of meander migration by bank failures, *J. Geophys. Res. Earth Surf.*, *119*, 1026–1042, doi:10.1002/2013JF002952.

Nikora, V., and A. G. Roy (2012), Secondary flows in rivers: Theoretical framework, recent advances and current challenges, in *Gravel Bed Rivers: Processes, Tools and Environments*, 2nd ed., edited by M. Church, P. Biron, and A. G. Roy, pp. 3–23, Wiley, Hoboken, N. J.

Nittrouer, J. A., D. Mohrig, M. A. Allison, and A.-P. B. Peyret (2011), The lowermost Mississippi River: A mixed bedrock-alluvial channel, *Sedimentology*, *58*, 1914–1934, doi:10.1111/j.1365-3091.2011.01245.x.

O'Neal, M. A., and J. E. Pizzuto (2011), The rates and spatial patterns of annual bank erosion revealed through terrestrial laser-scanner surveys of the South River, Virginia, *Earth Surf. Processes Landforms*, *36*, 695–701, doi:10.1002/esp.2098.

Papanicolaou, A. N., M. Elhakeem, and R. Hilldale (2007), Secondary current effects on cohesive river bank erosion, *Water Resour. Res.*, *43*, W12418, doi:10.1029/2006WR005763.

Parker, G., Y. Shimizu, G. V. Wilkerson, E. C. Eke, J. D. Abad, J. W. Lauer, C. Paola, W. E. Dietrich, and V. R. Voller (2011), A new framework for modeling the migration of meandering rivers, *Earth Surf. Processes Landforms*, *36*(1), 70–86, doi:10.1002/esp.2113.

Parsons, D. R., J. L. Best, R. J. Hardy, R. Kostaschuk, S. N. Lane, and O. Orfeo (2005), The morphology and flow fields of three-dimensional dunes, Rio Paraná, Argentina: Results from simultaneous multibeam echo sounding and acoustic Doppler current profiling, *J. Geophys. Res.*, *110*, F04S03, doi:10.1029/2004JF000231.

Parsons, D. R., P. R. Jackson, J. A. Czuba, F. L. Engel, B. L. Rhoads, K. A. Oberg, J. L. Best, D. S. Mueller, K. K. Johnson, and J. D. Riley (2013), Velocity Mapping Toolbox (VMT): A processing and visualization suite for moving-vessel ADCP measurements, *Earth Surf. Processes Landforms*, *38*(11), 1244–1260, doi:10.1002/esp.3367.

Przedwojski, B. (1995), Bed topography and local scour in rivers with banks protected by groynes, *J. Hydraul. Res.*, *33*, 257–273.

Reneau, S. ., P. G. Drakos, D. Katzman, D. V. Malmon, E. V. McDonald, and R. T. Ryti (2004), Geomorphic controls on contaminant distribution along an ephemeral stream, *Earth Surf. Processes Landforms*, *29*, 1209–1223, doi:10.1002/esp.1085.

Rhoads, B. L., and S. T. Kenworthy (1995), Flow structure at an asymmetrical stream confluence, *Geomorphology*, *11*(4), 273–293, doi:10.1016/0169-555X(94)00069-4.

Rozovskii, I. L. (1957), *Flow of Water in Bends of Open Channels*, pp. 233, Akad. Sci. Ukr. SRR, Kiev.

Szupiany, R. N., M. L. Amsler, J. L. Best, and D. R. Parsons (2007), Comparison of fixed- and moving-vessel flow measurements with an aDp in a large river, *J. Hydrol. Eng.*, *133*, 1299–1309, doi:10.1061/(ASCE)0733-9429(2007)133:12(1299).

Szupiany, R. N., M. L. Amsler, D. R. Parsons, and J. L. Best (2009), Morphology, flow structure, and suspended bed sediment transport at two large braid-bar confluences, *Water Resour. Res.*, *45*, W05415, doi:10.1029/2008WR007428.

Thorne, C. R. (1982), Processes and mechanisms of river bank erosion, in *Gravel-Bed Rivers*, edited by R. D. Hey, J. C. Bathurst, and C. R. Thorne, pp. 227–271, Wiley, Chichester, U. K.

Thorne, S. D., and J. D. Furbish (1995), Influences of coarse bank roughness on flow within a sharply curved fiver bend, *Geomorphology*, *12*, 241–257.

Vermeulen, B., M. G. Sassi, and A. J. F. Hoitink (2014), Improved flow velocity estimates from moving-boat ADCP measurements, *Water Resour. Res.*, *50*, 4186–4196, doi:10.1002/2013WR015152.Received.

Wood, A. L., A. Simon, P. W. Downs, and C. R. Thorne (2001), Bank-toe processes in incised channels: The role of apparent cohesion in the entrainment of failed bank materials, *Hydrol. Processes*, *15*(1), 39–61, doi:10.1002/hyp.151.

Yossef, M. F. M., and H. J. de Vriend (2011), Flow details near river groynes: Experimental investigation, *J. Hydraul. Eng.*, *137*, 504–516, doi:10.1061/(ASCE)HY.1943-7900.

Zinger, J. A., B. L. Rhoads, and J. L. Best (2011), Extreme sediment pulses generated by bend cut-offs along a large meandering river, *Nat. Geosci.*, *4*, 675–678, doi:10.1038/NGEO1260.